Your dedication goes here

Preface

Here come the golden words

place(s),
month year

Firstname Surname
Firstname Surname

Contents

List of Contributors

Christopher K. Anand McMaster University, 1280 Main Street West, Hamilton, Ontario, Canada, L8S 4K1
anandc@mcmaster.ca

Stephen J. Stoyan
University of Toronto, 5 King's College Road, Toronto, Ontario Canada, M5S 3G8
stoyan@mie.utoronto.ca

Tamás Terlaky McMaster University, 1280 Main Street West, Hamilton, Ontario, Canada, L8S 4K1
terlaky@mcmaster.ca

Author Name
University/Institute Name Street No. X - Place, Postal Code
name@e-mail.*

Author Name
University/Institute Name Street No. X - Place, Postal Code
name@e-mail.*

Author Name
University/Institute Name Street No. X - Place, Postal Code
name@e-mail.*

Author Name
University/Institute Name Street No. X - Place, Postal Code
name@e-mail.*

Author Name
University/Institute Name Street No. X - Place, Postal Code
name@e-mail.*

Author Name
University/Institute Name Street No. X - Place, Postal Code
name@e-mail.*

Author Name
University/Institute Name Street No. X - Place, Postal Code
name@e-mail.*

Author Name
University/Institute Name Street No. X - Place, Postal Code
name@e-mail.*

Author Name
University/Institute Name Street No. X - Place, Postal Code
name@e-mail.*

Author Name
University/Institute Name Street
No. X - Place, Postal Code
name@e-mail.*

Author Name
University/Institute Name Street
No. X - Place, Postal Code
name@e-mail.*

Author Name
University/Institute Name Street
No. X - Place, Postal Code
name@e-mail.*

Author Name
University/Institute Name Street
No. X - Place, Postal Code
name@e-mail.*

Author Name
University/Institute Name Street
No. X - Place, Postal Code
name@e-mail.*

Author Name
University/Institute Name Street
No. X - Place, Postal Code
name@e-mail.*

Author Name
University/Institute Name Street
No. X - Place, Postal Code
name@e-mail.*

Author Name
University/Institute Name Street
No. X - Place, Postal Code
name@e-mail.*

Author Name
University/Institute Name Street
No. X - Place, Postal Code
name@e-mail.*

Author Name
University/Institute Name Street
No. X - Place, Postal Code
name@e-mail.*

Part I

Part Title

The gVERSE RF Pulse: An Optimal Approach to MRI Pulse Design

Christopher K. Anand[1] Stephen J. Stoyan[2] and Tamás Terlaky[3]

[1] McMaster University, Hamilton, Ontario, Canada. anandc@mcmaster.ca
[2] University of Toronto, Toronto, Ontario, Canada. stoyan@mie.utoronto.ca
[3] McMaster University, Hamilton, Ontario, Canada. terlaky@mcmaster.ca

Summary. A Variable Rate Selective Excitation (VERSE) is a type of Radio Frequency (RF) pulse that reduces the Specific Absorption Rate (SAR) of molecules in a specimen. As high levels of SAR lead to increased patient temperatures during Magnetic Resonance Imaging (MRI) procedures, we develop a selective VERSE pulse that is designed to minimize SAR while preserving its duration and slice profile; called the generalized VERSE (gVERSE). After the formulation of a rigorous mathematical model, the nonlinear gVERSE optimization problem is solved via an optimal control approach. Using the state of the art Sparse Optimal Control Software ($\mathbb{SOCS}$), two separate variations of SAR reducing gVERSE pulses were generated. The Magnetic Resonance (MR) signals produced by numerical simulations were then tested and analyzed by an MRI simulator. Computational experiments involved with the gVERSE model provided constant RF pulse levels and had encouraging results with respect to MR signals. The testing results produced by the gVERSE pulse illustrate the potential advanced optimization techniques have in designing RF sequences.

1 Introduction to the Problem

Magnetic Resonance Imaging (MRI) produces high resolution cross-sectional images by utilizing selective Radio Frequency (RF) pluses and field gradients. Selective excitations are obtained by applying simultaneous gradient waveforms and a RF pulse with the appropriate bandwidth [LL01]. Many conventional RF pulse sequences are geared towards generating high definition images, but fail to consider the SAR (Specific Absorption Rate) of the excitation. High levels of SAR during MRI procedures can cause undesired side effects such as skin burns. Thus, one needs to reduce SAR levels and this is the focus of our paper. Instead of using common approaches to approximating the Bloch equation, we integrate the Bloch equation in a nonlinear optimization model that is designed to minimize RF SAR levels.

Several researchers have studied the selective RF excitation problem and employed different optimization methods in their designs. Simulated annealing

[She01], evolutionary algorithms [WXF91], quadratic optimization [CGN88] and optimal control techniques [CNM86, UGI04] are the most common. Although they produce solutions that relate to their desired profile, they are computationally intensive and in many cases their design for the pulse-envelope consists of relaxed conditions. In [UGI04], the excitation design under the optimal control approach leads to an ill-conditioned algebraic problem, which stems from the models attempt to include the Bloch equation in the Chebyshev domain. In [CGN88], Conolly *et al.* design the Variable Rate Selective Excitation (VERSE) pulse that is aimed at reducing MRI SAR levels; however, their model does not incorporate penalties to trade off energy and adhesion to the desired slice profile, nor does it incorporate relaxation.

The problem still remains, as pointed out in [CNM86, CGN88]. There is no sufficient mathematical formulation for pulse-envelope design. In this paper we address this problem, and use our model to construct a dynamical nonlinear optimization algorithm that is aimed at reducing RF SAR levels. Using Conolly's *et al.* idea, we design the generalized VERSE (gVERSE) pulse. The gVERSE pulse is a highly selective pulse that differs from its originator with respect to how SAR is minimized. The prefix "g" was added to VERSE because our objective function directly encompasses the high demands of RF pulse levels by allowing the gradient waveform to freely vary. In addition, we have significantly increased the dynamics of the VERSE problem, added additional constraints, and enhanced the degrees of freedom. Using our RF pulse formulation, we develop two separate pulse sequences that include variable slice gradients (listed as future work in [UGI04]).

In this paper, we begin with a review of general RF pulse sequences that leads to the development of our new SAR reducing gVERSE pulse model. In Section 3, the gVERSE model is fully detailed and the accompanying Nonlinear Optimization (NLO) problem is formulated. The implementation issues involved in computing the gVERSE pulse are briefly described in Section 4. In Section 5, the computational results for the gVERSE pulse are shown for two different test cases. The results are graphically illustrated and then tested by an MRI simulation in Section 6, where they are analyzed and examined with respect to the MR signals they generate. Finally, in Section 7 we conclude on how our results and MRI simulations show that mathematical optimization can have a strong effect on improving RF pulse sequences.

2 MRI Background

To understand the implications and effects of the gVERSE pulse we will begin with a short outline of our notation and a review of two different types of RF pulse sequences. For more information with regards to the MR formulations and/or general RF pulses, one can refer to [Bus96, HBTV99, LL01].

To begin, we define the Bloch equation which provides the rate of magnetization $(d\overrightarrow{M}(t)/dt)$,

$$\frac{d\overrightarrow{M}(t)}{dt} = \gamma\overrightarrow{M}(t) \times \overrightarrow{B}(t) + \frac{1}{\tau_1}(M_0 - M_z(t))\widehat{z} - \frac{1}{\tau_2}\overrightarrow{M}_{\perp}(t),$$

where t is time, $\overrightarrow{B}(t)$ is the external magnetic field in the z-axis direction, γ is the gyromagnetic constant, and

$$\overrightarrow{M}(t) = \begin{bmatrix} M_x(t) \\ M_y(t) \\ M_z(t) \end{bmatrix}, \text{ and } \overrightarrow{M}_{\perp}(t) = \begin{bmatrix} M_x(t) \\ M_y(t) \\ 0 \end{bmatrix}$$

are respectively the net and transverse magnetization vectors. Furthermore, $\widehat{z}$ is the z-axis unit vector, M_0 is the initial magnetization in the $\widehat{z}$ direction, τ_1 is the spin-lattice interaction parameter and τ_2 is the spin-spin interaction parameter. In addition, we let

$$\overrightarrow{B}(t) = \begin{bmatrix} b_x(t) \\ b_y(t) \\ b_z(t) \end{bmatrix},$$

where $b_x(t)$, $b_y(t)$ and $b_z(t)$ are the external magnetization vector coordinates, which will be used in the formulation of the gVERSE pulse.

2.1 Generic RF pulse

When processing an image, a number of precise RF pulses are applied in combination with synchronized gradients in different dimensional directions. For a detailed analysis of this process one can look at [CDM90, HBTV99, LL01]. We would like to highlight that RF pulses are only aimed at a specific portion of the object or specimen that the user intends to image. In addition, the RF pulse is accompanied by a gradient waveform that is used to spatially modulate the signals orientation [Bus96]. There are many different techniques in which RF and gradient waveforms can generate useable signals. Gaussian and sinc pulses are two of the many RF pulse sequences used today. Figure 1 is an illustration of a slice select sinc pulse [HBTV99]. Sinc pulses are successful at exciting particular magnetization vectors into the transverse plane that generate signal readings, however, they fail to account for side effects such as SAR levels. The heating effect experienced by patients during MRI procedures is measured by the level of SAR, which is a direct result of the RF pulse used. The level of SAR becomes particularly important with pediatric patients and as a result the FDA has strict limitations on SAR; which subsequently restricts RF pulse potential and other elements involved in MRI procedures. In addition, as MRI researchers are constantly developing faster scanners, higher tesla magnets, enhanced software components and improved RF coils; they are all still limited by SAR levels. Hence, RF pulses that consider such a factor are in high demand.

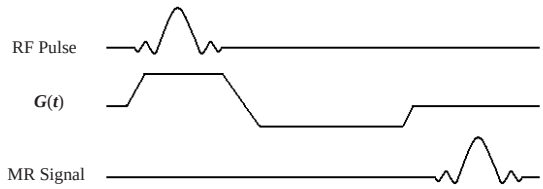

Fig. 1. A generic NMR slice select SINC pulse imaging sequence.

2.2 The VERSE Pulse

Originally proposed by Conolly *et al.* [CGN88], VERSE pluses were designed to generate MR signals similar to generic RF pulses, however, low pulse SAR levels were incorporated into the model. As mentioned, the SAR of a selective RF pulse is a critical parameter in clinical settings and may limit the use of a particular pulse sequence if the SAR limit exceeds given FDA requirements [LL01]. Due to the high SAR levels of various RF pluses the scan time for given pulse sequences are restricted [CGN88]. The key innovation with VERSE pulses is to allow a "trade off" between time and amplitude. By lowering RF pulse amplitude the duration of the pulse may be extended [CGN88]. As illustrated in Figure 2, VERSE pulses are similar to generic pulses, how-

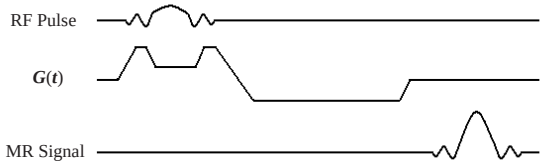

Fig. 2. The VERSE pulse imaging sequence.

ever, they contain a flattened center peak and their gradient waveform posses two additional steps. It is this uniform redistribution of the pulse area that allows the decrease in SAR. Conolly *et al.* designed three different types of SAR reducing pulses, each that had constraints on the strength of the RF pulse, however, they differed with respect to how they minimized SAR levels. The first model consisted of a minimum–SAR facsimile pulse for a specified duration, whereby the gradient waveform and RF pulse were integrated in the objective and subject to maximum gradient and constant duration constraints.

The second model used a minimum time formulation approach, whereby it searched for the briefest pulse that did not exceed a specified peak–RF level. The pulse was optimized for time and constrained by maximum gradient and RF levels. The final model, called the parametric gradient, constrained both the maximum gradient and slew-rate, and involved the parametric gradient and the RF pulse in the objective [CGN88]. The first two models consisted of a maximum of $3\kappa + 1$ variables, where κ was the total number of samples or RF pulses. The final model involved $\kappa(p + 1) + 1$ variables, where p represented the dimension of a parameter vector. Experimentation proved that only 256 sample values were necessary, which kept the variable count relatively low [CGN88]. Of the three algorithms, the parametric formulation offered the most robust SAR minimization, however, the design still had areas for improvement as the results contained gradient and RF timing mismatches. Subsequently, further experimentation was necessary with VERSE pulses, as Conolly *et al.* were the first to introduce this innovative concept.

3 The gVERSE Model

Conolly *et al.* [CGN88] showed that SAR can be reduced by combined RF/gradient reductions and time dilations, starting with an initial pulse design. For our research we would like to search a larger parameter space by allowing arbitrary gradient waveforms (subject to machine constraints), including sign changes. The gVERSE pulse is illustrated in Figure 3; our aim is to lower RF pulse energy and more evenly distribute the RF pulse signal. This flattened redistribution of the pulse will allow for a longer signal reading

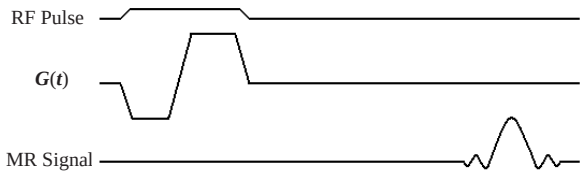

Fig. 3. The gVERSE pulse imaging sequence.

and potentially cause an even greater decrease in the level of SAR than the original VERSE pulse. Mathematically, this is the same as minimizing the external magnetic field generated by the RF pulse ($\overrightarrow{B}_{\mathrm{rf}}(t)$), and therefore our objective is

$$\min \text{SAR} = \int_0^T |\overrightarrow{B}_{\text{rf}}(t)|^2 dt = \int_0^T b_x^2(t) + b_y^2(t) dt,$$

where T is the time at the end of the RF pulse and

$$\overrightarrow{B}_{\text{rf}}(t) = \begin{bmatrix} b_x(t) \\ b_y(t) \\ 0 \end{bmatrix}.$$

As MRI is based on the interaction of nuclear spin with an external magnetic field, $\overrightarrow{B}_{\text{rf}}(t)$ is simply the vertical and horizontal components of $\overrightarrow{B}(t)$. Also, if low pulse amplitudes are produced by the gVERSE pulse, the duration T of the pulse can be increased.

Another part of MRI comes from the fact that since all magnetization vectors are spinning, there exists a rotational frame of reference. If we set up our equations in the rotating frame of reference then we exclude the uniform magnetic field generated by the main super-conducting magnet, B_0. Instead, we are left with the magnetic field of our RF pulse, $\overrightarrow{B}_{\text{rf}}(t)$, and our gradient

$$\overrightarrow{G}(t, s) = \begin{bmatrix} 0 \\ 0 \\ sG(t) \end{bmatrix},$$

where $sG(t)$ is the gradient value at coordinate position s. The primary function of the gradient is to produce time-altering magnetic fields such that the MR signal can be spatially allocated [HBTV99]. Hence, different parts of a specimen experience different gradient field strengths. Thus, by multiplying a constant gradient value by different coordinate positions s, we have potentially produced an equivalent linear relationship to what is used in practice. Fundamentally, coordinate positions s split a specimen or object into "planes" or "slices" along the s direction, which for the purposes of this paper will be parallel to $\widehat{z}$, as depicted in Figure 4. Here, s corresponds to a specific coordi-

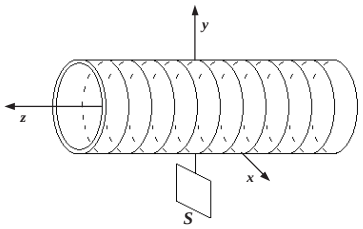

Fig. 4. Specimen or object separated into planes or slices about the z-axis.

nate value depending on its respective position and further it has a precise and

representative gradient strength. A RF pulse excites particular magnetization vectors into the transverse (x, y) plane where a signal is generated that is eventually processed into an image. In MRI a voxel corresponds to the unit volume of protons necessary to produce graphic information [HBTV99], and as this is directly related to a group or unit volume of magnetization vectors we will use the word voxel and magnetization vector interchangeably. Thus, s allows us to distinguish between voxels that are excited into the transverse plane by a RF pulse and those that are not. Coordinate positions, s, of voxels that are excited into the transverse plane will be recorded and referred to as being "in the slice." Magnetization vectors that are not tipped into the transverse plane will be referred to as being "outside the slice." Since any specimen or object we intend to image will have a fixed length, given $s \in S$, we will restrict S by choosing a finite set $S \subset \mathbb{R}$. S can then be further partitioned into the disjoint union of sets $S_{\text{in}} \cup S_{\text{out}}$, where S_{in} represents the coordinate positions in the slice and S_{out} represents the positions together with the magnetization vectors that we do not wish to tip into the transverse plane, i.e. those which are outside the slice. For each coordinate position $s \in S$ we add constraints corresponding to the Bloch equation, however, boundary constraints correspond to different conditions depending on the position of the slice, as we will discuss later. Fundamentally, voxels in S_{in}, ensure uniform magnetic tipping into the transverse plane, whereas $s \in S_{\text{out}}$, certify that external magnetization is preserved.

Thus, we now have the magnetic field $\overrightarrow{B}(t, s)$ with respect to coordinate positions s, whereby $b_x(t)$ and $b_y(t)$ are independent of s, hence

$$\overrightarrow{B}(t, s) = \overrightarrow{B}_{\text{rf}}(t) + \overrightarrow{G}(t, s).$$

Also, since $\overrightarrow{B}(t, s)$ has divided the $\widehat{z}$ component of our external magnetization into coordinate components, the same notation must be introduced into our net magnetization. By adding coordinate positions s to the magnetization vector we have,

$$\overrightarrow{M}(t, s) = \begin{bmatrix} M_x(t, s) \\ M_y(t, s) \\ M_z(t, s) \end{bmatrix}.$$

In addition, since VERSE pulses typically have short sampling times we will assume the same for the gVERSE pulse and thus omit proton interactions and relaxation. Therefore, including positions s into the Bloch equation, we are left with

$$\frac{d\overrightarrow{M}(t, s)}{dt} = \gamma \overrightarrow{M}(t, s) \times \overrightarrow{B}(t, s).$$

Hence, we have

$$\overrightarrow{M}(t, s) \times \overrightarrow{B}(t, s) = \begin{bmatrix} 0 & -sG(t) & b_y(t) \\ sG(t) & 0 & -b_x(t) \\ -b_y(t) & b_x(t) & 0 \end{bmatrix} \begin{bmatrix} M_x(t, s) \\ M_y(t, s) \\ M_z(t, s) \end{bmatrix},$$

and finally

$$\frac{d\overrightarrow{M}(t,s)}{dt} = \gamma \begin{bmatrix} 0 & -sG(t) & b_y(t) \\ sG(t) & 0 & -b_x(t) \\ -b_y(t) & b_x(t) & 0 \end{bmatrix} \overrightarrow{M}(t,s). \tag{1}$$

When stimulating a specific segment of a specimen by a RF pulse, some of the magnetization vectors are fully tipped into the transverse plane, partially tipped, and those lying outside the slice profile are minimally affected. The magnetization vectors that are only partially tipped into the transverse plane are described as having off-resonance and tend to disrupt pulse sequences and distort the final MRI image [HBTV99]. In anticipation of removing such inhomogeneities we introduce the angle α, at which net magnetization moves from the $\widehat{z}$ direction to the transverse plane. By convention, α will be the greatest at the end of our RF pulse, at time T, and since we are in the rotating frame we can remove the y-axis from our equations. Thus, we can eliminate off-resonance s coordinates by bounding voxels affected by the pulse

$$\left\| \begin{bmatrix} M_0 \sin(\alpha) \\ 0 \\ M_0 \cos(\alpha) \end{bmatrix} - \begin{bmatrix} M_x(T,s) \\ M_y(T,s) \\ M_z(T,s) \end{bmatrix} \right\| \leq \varepsilon_1,$$

and those in S_{out}, with $\alpha = 0$, hence

$$\left\| \begin{bmatrix} 0 \\ 0 \\ M_0 \end{bmatrix} - \begin{bmatrix} M_x(T,s) \\ M_y(T,s) \\ M_z(T,s) \end{bmatrix} \right\| \leq \varepsilon_2,$$

where $\varepsilon_1, \varepsilon_2 \geq 0$. By comparing these two bounds we can determine the s coordinates from which we would like the signal to be generated and exclude off-resonance.

Another factor we must integrate into our pulse is slew rate $W(t)$, also called gradient rise time. This identifies how fast a magnetic gradient field can be ramped to different gradient field strengths [CGN88]. As a result, higher slew rates enable shorter measurement times since the signal generated by the RF pulse to be imaged is dependent on it. Thus, the slew rate and gradient field strength together determine an upper bound on the speed and ultimately minimum time needed to perform the pulse. Thus, there must be a bound on these two entities in our constraints,

$$\begin{aligned} |G(t)| &\leq G_{\max}, \\ W(t) = \left| \frac{dG(t)}{dt} \right| &\leq W_{\max} \, . \end{aligned}$$

Finally, we have the semi-infinite nonlinear optimization problem

$$\min \text{ SAR} = \int_0^T b_x^2(t) + b_y^2(t) dt \, , \tag{2}$$

subject to,

$$\frac{d\overrightarrow{M}(t,s)}{dt} = \gamma \begin{bmatrix} 0 & -sG(t) & b_y(t) \\ sG(t) & 0 & -b_x(t) \\ -b_y(t) & b_x(t) & 0 \end{bmatrix} \overrightarrow{M}(t,s), \tag{3}$$

$$\left\| \begin{bmatrix} M_0\sin(\alpha) \\ 0 \\ M_0\cos(\alpha) \end{bmatrix} - \begin{bmatrix} M_x(T,s) \\ M_y(T,s) \\ M_z(T,s) \end{bmatrix} \right\| \leq \varepsilon_1, \tag{4S_{in}}$$

$$\left\| \begin{bmatrix} 0 \\ 0 \\ M_0 \end{bmatrix} - \begin{bmatrix} M_x(T,s) \\ M_y(T,s) \\ M_z(T,s) \end{bmatrix} \right\| \leq \varepsilon_2, \tag{4S_{out}}$$

$$|G(t)| \leq G_{\max}, \tag{5}$$

$$\left| \frac{dG(t)}{dt} \right| \leq W_{\max}, \tag{6}$$

$$M_x(0,s) = 0, \quad M_y(0,s) = 0, \quad M_z(0,s) = M_0, \tag{7}$$

where equations (2) – (7) hold for $\forall\, s \in S, t \in [0,T]$. Thus, depending on our bound for the pulse, we will construct two sets of constraints, one for the voxels $S_{\text{in}} \subset \mathbb{R}$ that will be excited by the RF pulse and one for those that will not, $S_{\text{out}} \subset \mathbb{R}$. Which indices are affected will be determined by the constraints ($4S_{\text{in}}$) and ($4S_{\text{out}}$).

3.1 Discretization

By separating our specimen into coordinate positions we have ultimately created two dimensional segments that are similar to records in a record box, whereby $s \in S$ represents the transverse plane at a particular position. Now we will discretize S into coordinate positions $s_1, s_2, \ldots, s_n$, where n is the total number of slices. As we have discussed earlier, S_{in} is the coordinate positions whose magnetization vectors have been tipped into the transverse plane by a RF pulse. Next we can define the finite band of particular coordinate positions in S_{in} to consist of positions $s_k, \ldots, s_{k+\delta}$, where $1 < k \leq k + \delta < n$, $\delta \geq 0$ and $k, \delta \in \mathbb{Z}$. Subsequently S_{out}, which was defined as positions that were not excited in the transverse plane, will consist of all coordinate positions not in S_{in}, hence, $S_{\text{out}} = s_1, \ldots, s_{k-1}, s_{(k+\delta)+1}, \ldots, s_n$. Figure 5 represents how $s_i \in S$ for $i = 1, \ldots, n$ would separate magnetization vectors into coordinate positions that have been tipped into the transverse plane, and those that have not. One should also note that we have only discretized with respect to coordinate positions $s_i \in S$, not time t. Furthermore, we will define the first coordinate position in S_{in} where RF pulse stimulation begins as $\underline{s}$, and similarly, the last position in S_{in} where stimulation ends as $\overline{s}$. Thus, we have $\underline{s} = s_k$ and $\overline{s} = s_{k+\delta}$, and we can now state the coordinate positions in the

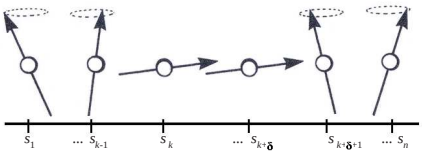

Fig. 5. Separating magnetization vectors into coordinate positions which are in the slice, S_{in}, and out, S_{out}.

slice as $S_{\text{in}} = [\underline{s}, \overline{s}]$. The first position where RF stimulation is a minimum, closest to $\underline{s}$, but in S_{out} and towards the direction of s_1, will be defined as $\underline{s}_l$. As well, the same will be done for the position closest to $\overline{s}$, which is in S_{out} and towards the direction of s_n, defined as $\overline{s}_u$. Consequently, $\underline{s}_l = s_{k-1}$ and $\overline{s}_u = s_{(k+\delta)+1}$, and therefore the coordinate positions outside the slice can be represented as $S_{\text{out}} = [s_1, \underline{s}_l] \cup [\overline{s}_u, s_n]$. As depicted in Figure 5, S_{in} is located between the two subintervals of S_{out}, where $s_i \in S_{\text{in}}$ is centered around 0, leaving S_{out} subintervals, $[s_1, \underline{s}_l] < 0$ and $[\overline{s}_u, s_n] > 0$. As well, $[s_1, \underline{s}_l]$ and $[\overline{s}_u, s_n]$ are symmetric with respect to each other, hence, the length of these subintervals are equivalent, $s_{k-1} - s_1 = s_n - s_{(k+\delta)+1}$. Furthermore, the difference between respective coordinate positions within each interval are equal to one another such that,

$$\begin{aligned} s_2 - s_1 &= s_n - s_{n-1} \\ s_3 - s_2 &= s_{n-1} - s_{n-2} \\ \vdots \qquad &\qquad \vdots \\ s_{k-1} - s_{k-2} &= s_{(k+\delta)+2} - s_{(k+\delta)+1}. \end{aligned} \tag{11}$$

Also note that the discretization points, s_i, within any interval $[s_1, \underline{s}_l], [\underline{s}, \overline{s}]$ and $[\overline{s}_u, s_n]$ do not necessarily have to be uniformly distributed and thus, more or less coordinate positions can be positioned closer to the boundaries of S_{in} and S_{out}. The distance between coordinate positions $(\underline{s}_l, \underline{s})$ and $(\overline{s}, \overline{s}_u)$ will be much larger in comparison to other increments of s_i. This is typically the area where voxels that have off-resonance characteristics are located. As mentioned earlier, magnetization vectors having off-resonance tend to disrupt pulse sequences and distort the MRI image. For this reason we will define tolerance gaps S_0 of finite length between $(\underline{s}_l, \underline{s})$ and $(\overline{s}, \overline{s}_u)$, where off-resonance prominently resides. Hence, S can now be partitioned into $S_{\text{in}} \cup S_{\text{out}} \cup S_0$ where a general sequence of the intervals would be $S_{\text{out}}, S_0, S_{\text{in}}, S_0, S_{\text{out}}$.

3.2 gVERSE Penalty

An important component of the model now becomes evident, the nonlinear optimization problem defined in (2) – (7) may be infeasible or difficult to solve

as the number n of $s_i \in S$ becomes large and the slices are close together. In particular, constraints $(4S_{\text{in}})$ and $(4S_{\text{out}})$ pose a threat to the feasibility of the problem as the number of discretization points increase. A penalty for the violation of these constraints can be imposed such that an optimal solution is located for problems with large numbers of variables and small distances between s_i coordinate positions. The basic idea in penalty methods is to relax particular constraints and add a penalty term to the objective function that prescribes high cost to infeasible points [Ber95]. The penalty parameter determines the severity of violation and as a consequence, the extent to which the resulting unconstrained problem approximates the original constrained one. Thus, returning to the semi-infinite nonlinear optimization problem formulated at the start of Section 3, we introduce penalty variables ξ_1 and ξ_2 to constraints $(4S_{\text{in}})$ – $(4S_{\text{out}})$, and the optimization problem objective becomes

$$\min \text{SAR} = \int_0^T b_x^2(t) + b_y^2(t)\, dt + \xi_1\zeta_1 + \xi_2\zeta_2, \tag{12}$$

subject to constraints (3), (5) – (7), and

$$\left\| \begin{bmatrix} M_0\sin(\alpha) \\ 0 \\ M_0\cos(\alpha) \end{bmatrix} - \begin{bmatrix} M_x(T,s_i) \\ M_y(T,s_i) \\ M_z(T,s_i) \end{bmatrix} \right\| \leq \varepsilon_1 + \xi_1, \tag{13S_{in}}$$

$$\left\| \begin{bmatrix} 0 \\ 0 \\ M_0 \end{bmatrix} - \begin{bmatrix} M_x(T,s_i) \\ M_y(T,s_i) \\ M_z(T,s_i) \end{bmatrix} \right\| \leq \varepsilon_2 + \xi_2, \tag{13S_{out}}$$

where $\zeta_1, \zeta_2 \in \mathbb{R}$ are scalar penalty parameters and as in the earlier equations of Section 3, (12) – $(13S_{\text{out}})$ apply $\forall\, s \in S$, $t \in [0,T]$. One should note that the larger the value of ζ_1 and ζ_2, the less violated constraints $(13S_{\text{in}})$ and $(13S_{\text{out}})$ become. In addition, as it is written the penalty variables are applied to each $s_i \in S$ for constraints $(13S_{\text{in}})$ and $(13S_{\text{out}})$. However, depending on computational results, it may be appropriate to only penalize coordinate positions in the neighbourhood of the bounds $[\underline{s}_l, \underline{s}]$ and $[\overline{s}, \overline{s}_u]$. This would enhance the constraints on the optimization problem and only allow violations to occur at the most vulnerable points of the problem. Adding penalty variables and parameters to our optimization problem is an option that may not be necessary. It is dependent on the number n of coordinate positions applied to the model as well as how close we would like $s_i \in S$ to be to one another. Hence, for the remainder of this paper we will omit writing out the penalty variables and parameters, however, the reader should note that they can easily be incorporated into the formulation.

4 Results

The gVERSE pulse was designed to improve RF pulse sequences by minimizing SAR levels while upholding MRI resolution, however, the complex math-

ematical requirements of the model may be difficult to satisfy. Even simple NLO problems with large numbers of variables can be challenging to solve and threatens many software packages. Thus, when attempting to minimize the objective function in (2) under the constraints (3) – (7), the number of variables implemented was especially important. Preliminary results were found by implementing the gVERSE model using five coordinate positions and the SQP based Optimal Control software package SOCS solved the demanding time dependent NLO problems. This kept the variable count to a minimum of 19 $(3n + 4)$, excluding the independent time variable t. The number of slices were systematically increased until software limitations on memory became a factor. Nonetheless, this was a remarkably larger number of variables than anticipated as it accounted for 15 slices with a total of 38 857 variables. By experimenting and consulting the literature, realistic MRI values for the constants were used during each computation. Namely, $\gamma = 42.58$ Hz/mT, $G_{\max} = 0.02$ mT/mm and $W_{\max} = 0.2$ mT/mm/ms, where Hz is Hertz, mm is millimeters, ms is milliseconds, and mT is millitelsa. The magnetization vectors in S_{in} were fully tipped into the transverse plane, hence, $\alpha = \pi/2$. The magnitude of the initial magnetization vector for each coordinate position had an initial magnetization value of $M_0 = 1.0$ spin density units. Initially, we chose $\varepsilon_1, \varepsilon_2 \leq 0.1$, however, as the number of variables increased for the problem, the larger the value of ε_1 and ε_2 had to be in order to find a feasible solution, hence, $\varepsilon_1, \varepsilon_2 = 0.1$ for the 15 slice results.

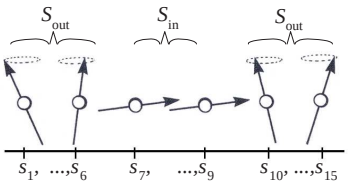

Fig. 6. The separation of coordinate positions s_i into S_{in} and S_{out} for 15 magnetization vectors.

4.1 Fifteen Slice Results

The results for the 15 slice problem accounted for the largest number of variables that $\mathbb{SOCS}$ could solve. The problem became even more challenging as the distance from $\underline{s}$ to $\underline{s}_l$ and $\overline{s}$ to $\overline{s}_u$ decreased. For smaller distances between the magnetization vectors in S_{in} and S_{out} penalty variables and parameters had to be incorporated into the formulation of the problem. We will begin with the 15 slice results without penalty, where a greater distances between $\underline{s}$ to $\underline{s}_l$ and $\overline{s}$ to $\overline{s}_u$ were used.

Since there were 15 slices, the three middle magnetization vectors were tipped into the transverse plane to ensure that the symmetric structure of the problem was maintained. Hence, coordinate positions s_7, s_8 and s_9 were in S_{in}, while s_1, $s_2, \ldots$ s_6 and s_{10}, $s_{11}, \ldots$ s_{15} remained in S_{out}. The arrangement of the coordinate positions is shown in Figure 6 and the exact values for the coordinate positions are as follows:

$$\begin{array}{cccccccccccccccc} -30 & -28 & -26 & -24 & -22 & -20 & -0.2 & 0 & 0.2 & 20 & 22 & 24 & 26 & 28 & 30 \\ s_1 & s_2 & s_3 & s_4 & s_5 & s_6 & s_7 & s_8 & s_9 & s_{10} & s_{11} & s_{12} & s_{13} & s_{14} & s_{15} \end{array}$$

which is in mm. The results for the 15 slice coordinate simulation is illustrated in Figures 7, 8 and 11. Information on the magnetic vector projection is shown in the graphs found in Figures 7 – 8. Due to the symmetric structure of the problem, voxels $s_1, \ldots, s_6$ and $s_{10}, \ldots, s_{15}$ were identical, as were s_7 and s_9. Hence, only the first eight coordinate positions are shown. Thus, Figure 7 – 8 corresponds to magnetization vectors in S_{out} and S_{in}. The resulting RF

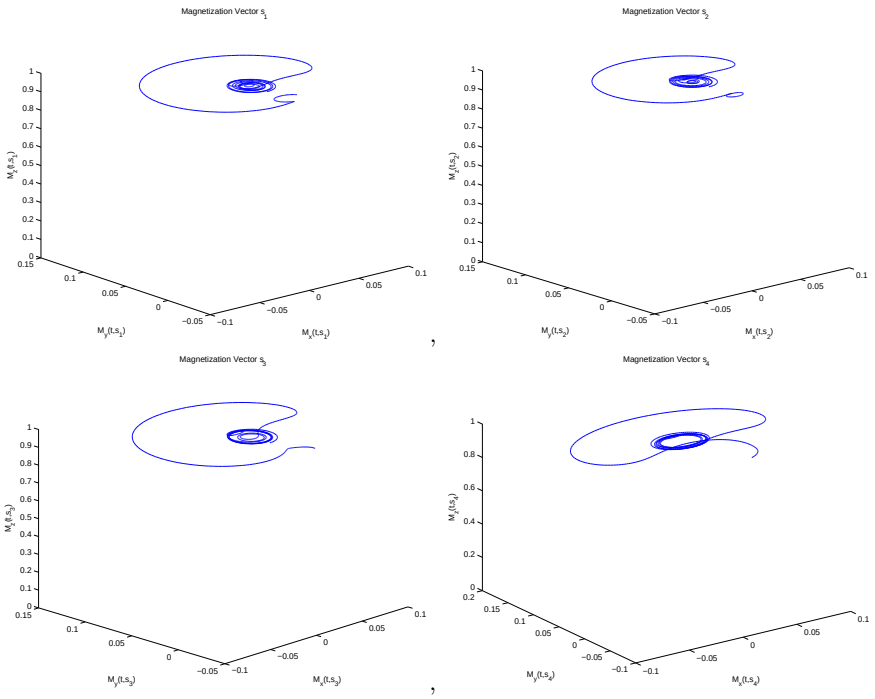

Fig. 7. From Top to bottom, magnetization vectors corresponding to coordinate positions s_1, s_2, s_3 and s_4.

pulse procedure, represented by the external magnetization components and

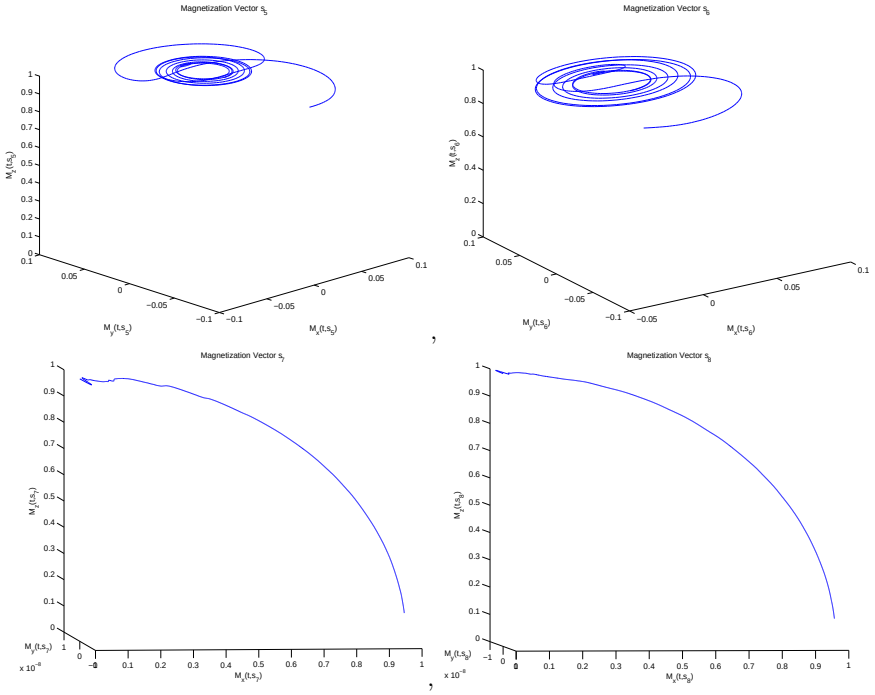

Fig. 8. From top to bottom, magnetization vectors corresponding to coordinate positions s_5, s_6, s_7 and s_8.

the gradient waveform is shown in Figure 11; $b_x(t)$ is not shown as it was constant and equal to zero.

One can observe that the precession of the magnetization vectors in S_{out} is evident, this is shown in the graphs of Figures 7 – 8. The initial point is close to the voxels precession range and at most it takes one full rotation for them to orbit uniformly. The magnetization vectors in Figure 8, those s_i that belong to S_{in}, smoothly tip into the transverse plane without any cusps or peaks. There are small differences between s_7 and s_8 as they begin to tip into the transverse plane, however, they act very similar after their height decreases below 0.8 spin density units. In Figure 11, the gradient waveform starts off negative and then ends up positive. It is not a smooth curve since it is composed of many local hills and valleys. Also, the gradient seems to be the opposite of what is used in practical MRI sequences, however this proves to be a proficient sequence as we will investigate in the next Section. Finally, the external magnetization components, $b_x(t)$ and $b_y(t)$, are constant and linear, precisely what we optimized for in the objective function. The value of $b_x(t)$ is zero mT/mm, while $b_y(t)$ of Figure 11 has a constant value of 0.01925 mT/mm.

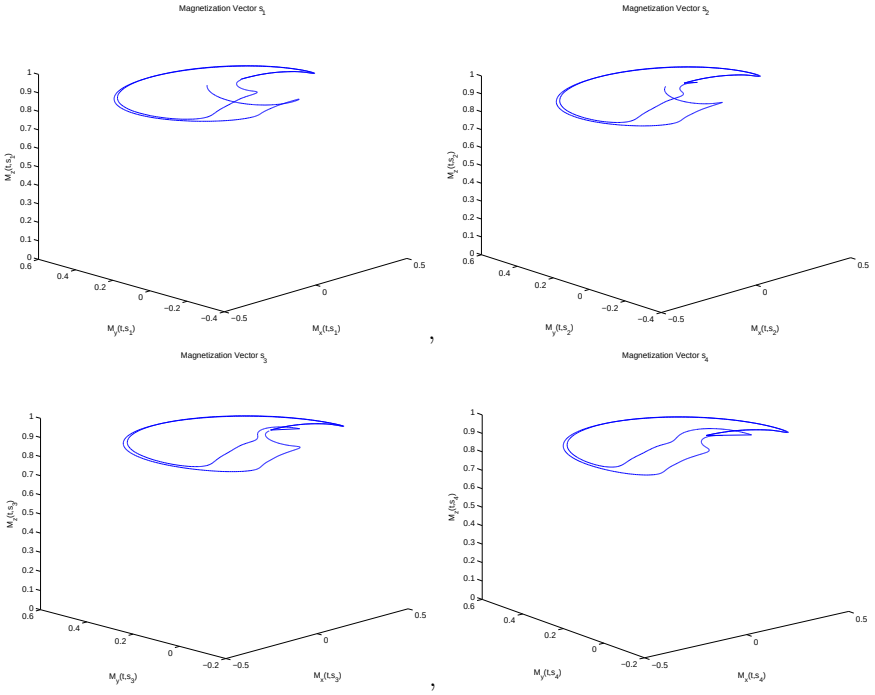

Fig. 9. From top to bottom, magnetization vectors corresponding to coordinate positions s_1, s_2, s_3 and s_4.

4.2 Fifteen Slice Penalty Results

To increase the distance between the coordinate positions that were tipped into the transverse plane and allow a smooth transition between magnetization vectors in S_{in} and S_{out}, penalty variables and parameters were introduced. As described in Section 3.2, penalty variables were added to each s_i vector in constraints $(13S_{\text{in}})$ and $(13S_{\text{out}})$ in order to decrease the distance between $[\underline{s}, \underline{s}_l]$ and $[\overline{s}, \overline{s}_u]$. The remaining variables, constants, and constraints were consistent with what was used in the 15 slice results. The exact values for the coordinate positions were as follows:

$$\begin{array}{cccccccccccccccc} -30 & -28 & -26 & -24 & -22 & -20 & -2 & 0 & 2 & 20 & 22 & 24 & 26 & 28 & 30 \\ s_1 & s_2 & s_3 & s_4 & s_5 & s_6 & s_7 & s_8 & s_9 & s_{10} & s_{11} & s_{12} & s_{13} & s_{14} & s_{15} \\ \xi_2 & \xi_2 & \xi_2 & \xi_2 & \xi_2 & \xi_2 & \xi_1 & \xi_1 & \xi_1 & \xi_2 & \xi_2 & \xi_2 & \xi_2 & \xi_2 & \xi_2 \end{array}$$

where the positions that were penalized have their respective penalty variables listed below them. Notice that with the addition of penalty variables and parameters the distance from s_7 to s_9 increased to 4 mm, compared to the 0.4 mm difference in the 15 slice results on page 15. This allowed the difference

between the vectors in S_{in} and S_{out} to be reduced. The results for the penalized 15 coordinate simulation is illustrated in Figures 9, 10 and 12, where the value of the penalty parameters were $\zeta_1 = 100$ and $\zeta_2 = 100$. The profiles of the magnetic moments are shown in Figures 9 – 10. Again, due to the problems symmetry we have omitted the graphs of the magnetization vectors corresponding to coordinate positions $s_9, \ldots, s_{15}$. Hence, Figure 9 and the top two graphs in 10 correspond to magnetization vectors in S_{out}, whereas the bottom two graphs in Figure 10 refer to the coordinate positions in S_{in}. The resulting RF pulse procedure, represented by the external magnetization components and gradient sequence is shown in Figure 12; again $b_x(t)$ is not shown as it was constant and equal to zero.

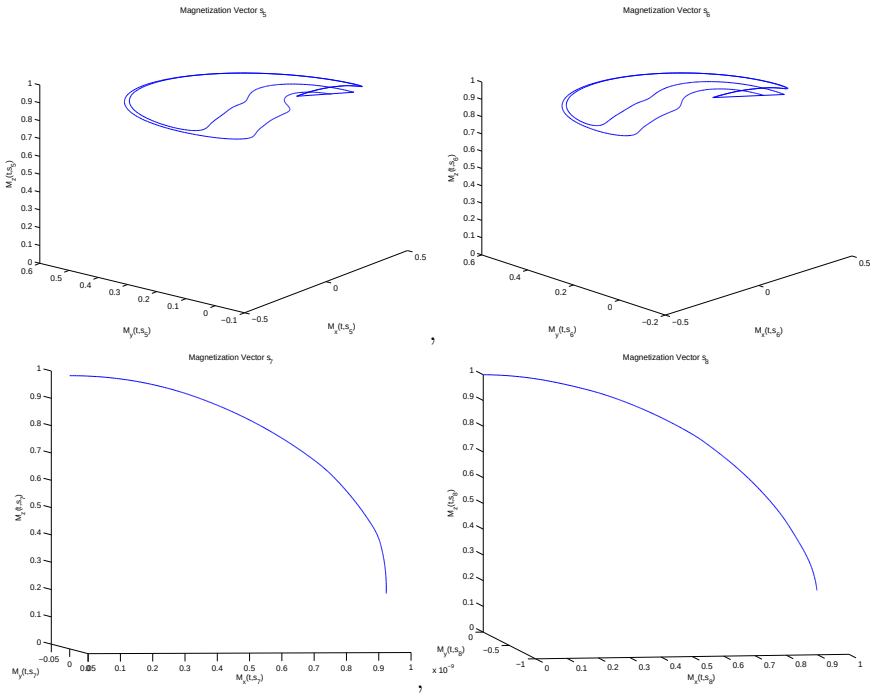

Fig. 10. From top to bottom, magnetization vectors corresponding to coordinate positions s_5, s_6, s_7 and s_8.

As illustrated, the precession of the magnetization vectors in S_{out}, Figures 9 – 10, have a much larger radius than that of the 15 slice problem. In fact, these magnetization vectors have at most three successive orbits in the entire time duration. The magnetization vectors in Figure 10, those s_i that belong to S_{in}, smoothly tip into the transverse plane and there is a greater similarity between s_7 and s_8 than in the preceding results. However, due to the penalty

variables these vectors only tip down to a spin density value of 0.2. Also, the y-axis is larger than was in the 15 slice problem, this is because the $M_y(t,\cdot)$ vectors are increasing as they descend into the transverse plane. In Figure 12, the gradient waveform contains two large peaks. The first is negative and it starts about one quarter into the time period. The second peak is positive and it starts approximately three quarters into the time period. Also, the gradient sequence has three linear segments. One that is zero at the start of the sequence and the other two occur within the peaks, each having a value of exactly $\pm G_{\max}$. For the external magnetization components, $b_x(t)$ is again constant and has a value of zero mT/mm. Although the axis of $b_y(t)$ in Figure 12 has been magnified, it is not as linear as the previous results and has increased to a value of approximately 0.10116 mT/mm. Nevertheless, this is still less than the amplitude for a conventional pulse, such as the one illustrated in Figure 1, which has a typical $b_y(t)$ value of approximately 0.7500 mT/mm. In fact, if we look at the value of the objective function in (2), the 15 slice penalty results have an objective value of 0.1874 SAR units, whereas the generic RF pulse produced a value of 0.5923 SAR units. The 15 slice results generated the lowest objective value of 0.0385 SAR units.

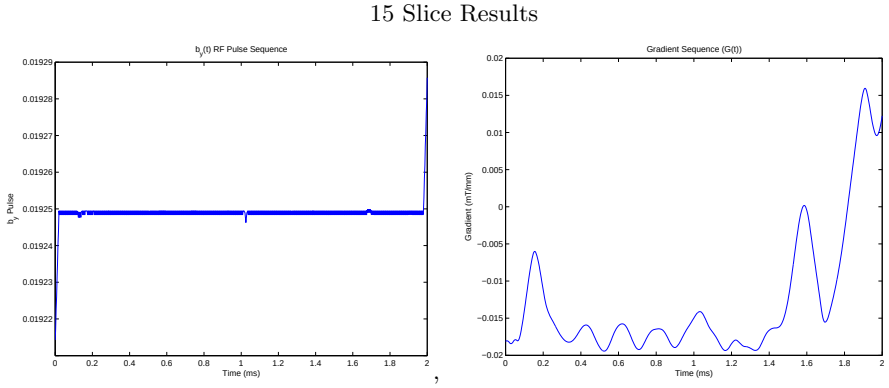

Fig. 11. External magnetization component $b_y(t)$ and gradient sequence $G(t)$ for the 15 slice results, $b_x(t)$ is zero.

Using the simulated gVERSE magnetization results, we produce two different graphs showing the transverse and longitudinal magnetization profiles. The desired magnetization distributions for a 90^0 RF pulse with 15 coordinate positions are shown in Figure 13, for further information about the desired profiles the reader may consult [CNM86], [HBTV99]. The transverse magnetization profile illustrated in Figure 14 is very similar to what is desired as given in Figure 13. The M_x magnetization component is free of ripples and contains the requested step function. The M_y magnetization profile is included to illustrate its minimal presence. One should note that the lower axis in Figures

15 Slice Penalty Results

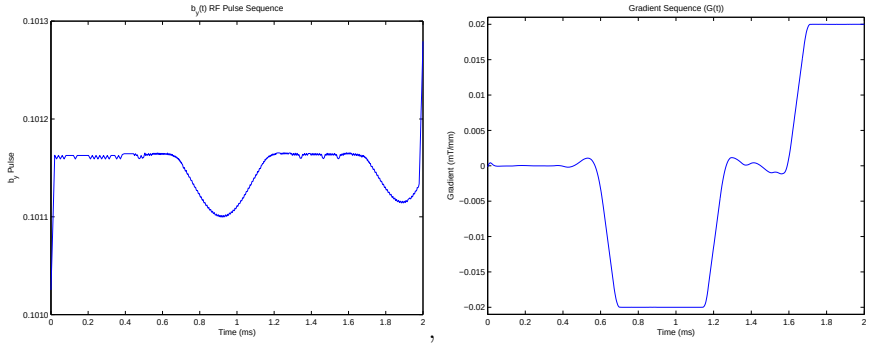

Fig. 12. External magnetization component $b_y(t)$ and gradient sequence $G(t)$ for the 15 slice penalty results, $b_x(t)$ is zero.

13 – 14 represents the magnetization vectors coordinate positions and from the results this corresponds to a distance of 60 mm. The longitudinal magnetization profile in Figure 14 is also similar to what is implored, however, the M_z dip is slightly higher than desired. In Figure 14 it is important to note that our resultant profiles have no ripples extending past the slice of interest, which is not the case for the results of [CNM86], [CGN88] and [UGI04]. By virtually omitting ripples in our magnetization profiles we potentially reduce aliasing and other such factors that disrupt MR image resolution.

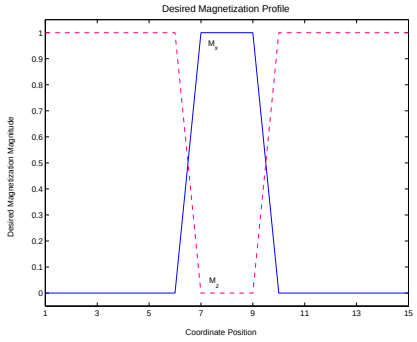

Fig. 13. Desired M_x and M_z distribution profiles for a 90^0 pulse.

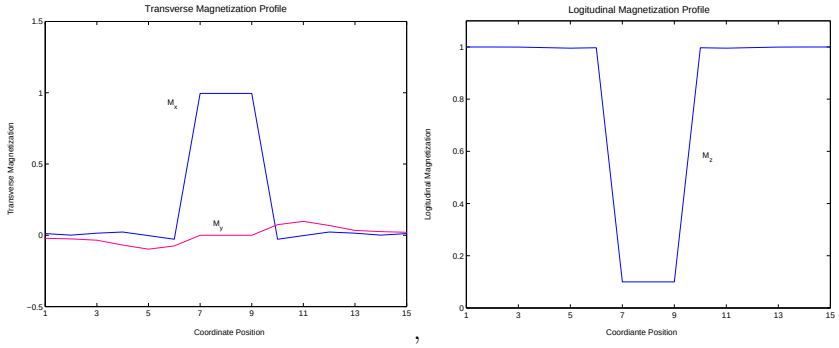

Fig. 14. Transverse magnetization components highlighting M_x and M_y magnitudes (left), Longitudinal M_z magnetization component magnitude (right).

5 Image Reconstruction

To obtain an idea of how the gVERSE pulse performs with respect to MR imaging, we provide a simple illustration of its behaviour. First, one should be familiar with how the signal produced by the RF pulse is mathematically amplified, digitized, transformed, and then combined together with other signals to form a final image [CDM90, HBTV99, LL01, Nis96]. There are several techniques that can be used to produce a final image, however, the core of the systematic procedure is the same for all methods. For the purpose of our analysis we use 1D imaging coverage.

5.1 gVERSE Simulation

An MRI simulation was implemented in Matlab to test the performance of the gVERSE pulse where using the Bloch equation we created an environment similar to that which is occurring in practical MRI. Thus, by feeding the optimized RF and gradient gVERSE values to a program that simulates the behaviour of a portion of a human spinal cord, we can show how the gVERSE MR signal performs. Specifically, the gVERSE values of $G(t_j)$, $b_x(t_j)$ and $b_y(t_j)$ for $j = 1, \ldots, N$ were read into the Bloch equation (1) for magnetization vectors at different $s_1, \ldots, s_n$ positions. Although we used a total of n coordinate positions in the optimization of our model, the RF pulse and gradient sequence can be applied to $> n$ positions for imaging purposes. Thus, given $\overline{n} > n$ coordinate positions, N time discretizations, the initial magnetization vector $(\overrightarrow{M}_0)$ in the $\widehat{z}$ direction, the Bloch equation was numerically integrated for each s_i value and $j = 1, \ldots, N$. The VESRE pulse sequence, $G(t_j), b_x(t_j)$ and $b_y(t_j)$, was then inserted into the integral of

$$\overrightarrow{M}(t, s_i) = \int_{t_1}^{t_N} \frac{d\overrightarrow{M}(\widehat{t}, s_i)}{dt}\, dt, \tag{31}$$

for $i = 1, \ldots, \overline{n}$ and where $\widehat{t} = [t_1, t_2, \ldots, t_N]^T$. The values for the magnetization vectors were then converted into a signal by simulating the amplification and digitization used in MRI. For a complete description of how (31) was integrated and amplified one can refer to [Sto04]. At this step we would be able to investigate the signal produced by our simulation and examine its properties.

Using the gVERSE gradient and RF pulse sequence many MRI simulations were conducted over various tissues. We will show one of the results, for more simulation examples the reader can see [Sto04]. As there was relatively no difference with regards to simulation results using either of the gVERSE cases, the 15 slice penalty results are shown as they were the better of the two. Using cerebrospinal fluid, the most graphically significant results were tested by placing the tissue on an angle, as shown in Figure 15. As the signal generated by the pulse has a direct relationship with that of the tissues spin density, each tissues spin density value was substituted into M_0 at its respective position. Thus, a spin density value of 1.0 for cerebrospinal fluid was used when performing the MR imaging simulation. Also note, the gVERSE pulse was designed to tip only the magnetization vectors in S_{in} into the transverse plane. Thus, the coordinate positions $s_i \in S_{\text{in}}$ would produce a peak in the signal when the gVERSE pulse reaches the cerebrospinal fluid for these $s_i \in S_{\text{in}}$ voxels. As detailed in the preceding sections, voxels $s_i \in S_{\text{in}}$ are located at the center coordinate positions, Figure 16.(A) represents the signal

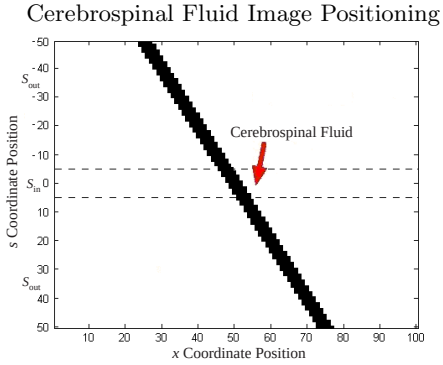

Fig. 15. The angular position of cerebrospinal fluid to be imaged by our MRI simulation.

generated after the gVERSE pulse and gradient waveform was used to excite particular voxels within the cerebrospinal fluid into the transverse plane. As it is shown in Figure 16.(A), the large central peak in the signal represents when the gVERSE pulse reaches the voxels in S_{in} of the fluid. The peak in the center of the figure is very distinctive and although noise was not integrated into the simulation, the signal produced a strong step function. Figure

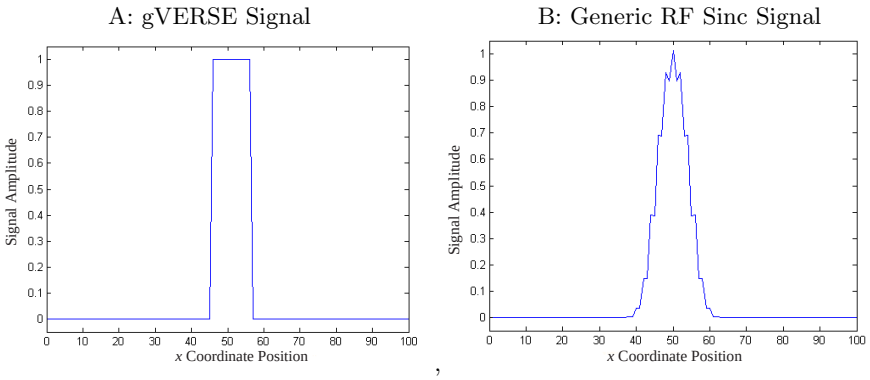

Fig. 16. The signal produced by the gVERSE pulse MRI simulation over the diagonal cerebrospinal fluid (A), and when a generic sinc RF pulse and gradient sequence is applied (B).

16.(B) represents the signal produced when a generic sinc pulse and gradient waveform is used. In comparing Figure 16.(A) to Figure 16.(B), one can see that the signal produced by the gVERSE pulse has a highly distinctive central peak and a much clearer division with regards to what is tissue and what is not. The base of the signal in Figure 16.(A) is also more representative of when the voxels in S_{in} reach the fluid, which is not the case for the sinc pulse. In addition, the objective value, which defines the strength of the RF pulse necessary to produce such a signal, was 0.1874 SAR units for the gVERSE pulse, substantially lower than that of the conventional pulse, which had an objective value of 0.5923 SAR units.

6 Conclusions and Future Work

We designed the gVERSE model to reduce the SAR of RF pulses by maintaining a constant RF pulse strength ($\overrightarrow{B}_{\text{rf}}$ value) and generating high quality MR signals. It was shown that the gVERSE results produced strong MR signals with clear divisions of the location of the tissue being imaged. For this reason various MRI studies utilizing gVERSE pulses could be developed in the near future.

The observations noted in Section 4 deserve some additional reasoning and explanation. To begin, the reader should understand that the symmetry displayed between coordinate position vectors in each of the result cases was precisely designed in (11) of the gVERSE model. However, the precession illustrated by the magnetization vectors was not directly part of the gVERSE design, it was a consequence of the Bloch constraint (3). Nonetheless, the precession shown in our results validated our design since it occurs within the nucleus of atoms in vivo. Furthermore, investigating the precession of the

magnetization vectors in the 15 slice results, it was shown that they had a much tighter radial orbit than the 15 slice penalty results. This was due to the fact that the penalty parameters allowed the feasible range of the constraints on these variables to be larger. With respect to precession, the 15 slice results were the most realistic. However, penalty variables in the 15 slice penalty results allowed the span of the magnetization vectors in S_{in} to be fairly large, which is probably what occurs in practice. In addition, investigating only the coordinate positions in S_{in} one should note that the penalty variables relaxed the constraints of the 15 slice penalty results, which did not induce the wave-like motion found in the vectors of the 15 slice results. One could conclude that in order to have improved transverse tipping and increase the length of magnetization vectors in S_{in}, larger ε_2 values are necessary, however, whether or not such a large precessional value is a realistic approximation would then become a factor.

The aim of the gVERSE pulse was to minimize SAR by maintaining a constant RF pulse ($b_x(t)$ and $b_y(t)$ values), which was established in both of the results. Although the values of $b_x(t)$ were identical for both cases, $b_y(t)$ values increased as the distance between the slices in S_{in} became larger. This was expected since an increase in the distance between $\overline{s}$ and $\underline{s}$ would require additional energy to tip the voxels into the transverse plane, yielding an increase in the strength of the RF pulse, or larger $b_y(t)$ value. The $b_y(t)$ values for the penalty results were the greatest and were not as constant as the other case. This was again due to the penalty variables and parameters, however, the nonlinear portions of the $b_y(t)$ graph only had small differences with respect to the other values; and they were lower. Also, when comparing the gVERSE pulse to conventional pulses the gVERSE objective value was lower for all cases, and hence, did not require as much energy to tip the magnetization vectors into the transverse plane. Finally, the most surprising part of the gVERSE pulse results is the gradient waveform. Since we optimized for the RF pulse in our model, this process returned the gradient waveform that would allow such a pulse to occur. In other words, in order to use the $b_x(t)$ and $b_y(t)$ pulse design, the accompanying gradient waveform, mainly derived from the Bloch constraint, would have to be imposed to acquire a useable signal. With regards to practical MR gradient waveforms, the 15 slice penalty results produced the simplest and most reasonable gradient vales to implicate, particularly due to its large linear portions. However, if necessary, regardless of the difficulty, either gradient could be implemented. Finally, both results had similar features in the sense that they each started off fairly negative and then ended up quite positive. This is a very interesting consequence of the gVERSE pulse, as shown in Section 2 and 4, conventional gradient sequences usually have the opposite characteristics. In terms of our MRI simulation, good signal results were produced for such unique gradient waveforms, which would justify further research with gVERSE pulses. In fact, Sections 5 and 6 demonstrated that the gVERSE RF pulse and gradient sequence were viable and could be applied to practical MRI.

Future Work

The gVERSE pulse proved to have encouraging MRI results and performed to be better than anticipated with respect to useable MR imaging signals. However, there are still areas left for investigation and various elements of the gVERSE model can be improved. A few of the issues that should be taken into account for future developments are:

- Specializing the model to the rotating structure of the equations;
- Apply the gVERSE model to more than 50 slices;
- Add spin-lattice and spin-spin proton interactions to the gVERSE formulation;
- Apply alternative optimization software to the problem;
- Include gradient distortions to the gVERSE model.

The issues are listed in sequential order, starting with what we believe is the most important item to be addressed. As most are self explanatory, adding rotation into the equations was one of the factors that deemed to be important after the results were examined. By integrating the rotating frame of reference into our equations we eliminated the y-axis. It is possible that this was a source of singularities when optimizing and therefore caused $\mathbb{SOCS}$ to increase the size of its working array, occasionally creating memory problems.

References

[Ber95] Bertsekas, D.P.: Nonlinear Programming. Athena Scientific, Belmont, Massachusetts (1995)

[Ber01] Betts, J.T.: Practical Methods for Optimal Control Using Nonlinear Programming. Society for Industrial and Applied Mathematics, Philadelphia (2001)

[BH01] Betts, J.T., and Huffman, W.P.: Manual: Release 6.2 M and CT-TECH-01-014. The Boeing Company, PO Box 3707. Seattle, WA 98124-2207 (2001)

[Bus96] Bushong, S.C.: Magnetic Resonance Imaging: Physical and Biological Principles. Mosby, Toronto, 2nd edition (1996)

[CNM86] Conolly, S.M., Nishimura, D. G., and Macovski, A.: Optimal Control Solutoins to the Magnetic Resonace Selelctive Excitation Problem. IEEE Transacitons on Medical Imaging, **MI-5**, 106-115 (1986)

[CGN88] Conolly, S.M., Glover, G., Nishimura, D.G., and Macovski, A.: Variable-Rate Selective Excitation. Journal of Magnetic Resonance, **78**, 440-458 (1988)

[CDM90] Curry, T.S., Dowdey, J.E., and Murry, R.C.: Christensen's Physics of Diagnostic Radiology. Lippincott Williams and Wilkins, New York, 4th edition (1990)

[HBTV99] Haacke, E.M., Brown, R.W., Thompson, M.R., and Venkatesan, R.: Magnetic Resonance Imaging: Physical Principles and Sequence Design, John Wiley and Sons, Toronto (1999)

[LL01] Liang, Z.P., and Lauterbur, P.C.: Principles of Magnetic Resonance Imaging: A Signal Processing Perspective. IEEE Press, New York, New York (2001)

[Nis96] Nishimura, D.G.: Principles of Magnetic Resonance Imaging. Department of Electrical Engineering, Stanford University, San Francisco (1996)

[She01] Shen, J.: Delayed-Focus Pulses Obtimized Using Simulated Annealing. Journal of Magnetic Resonance, **149**, 234-238 (2001)

[Sto04] Stoyan, S.J.: Variable Rate Selective Excitation RF Pulse in MRI. M.Sc. Thesis: McMaster University, Hamilton (2004)

[UGI04] Ulloa, J.L., Guarini, M., and Irarrazaval, P.: Chebyshev Series for Designing RF Pulses Employing an Optimal Control Approach. IEEE Transacitons on Medical Imaging, **23**, 1445-1452 (2004)

[WXF91] Wu, X.L., Xu, P., and Freeman, R.: Delayed-Focus Pulses for Magnetic Resonace Imaging: An Evolutionary Approach. Magnetic Resonance Medicine, **20**, 165-170 (1991)